Quantifying Cartilage Biomechanical Properties Using a Linearized Frequency-Domain Method

A. Gkousioudi,[1,2] D. S. Tzeranis,[1,3] G. P. Kanakaris,[1] M. Saloufas,[1] and L. G. Alexopoulos[1]

[1]Department of Mechanical Engineering, National Technical University of Athens, 157 80 Zografou, Greece; [2]School of Medicine, University of Patras, 265 04 Rio Achaias, Greece; and [3]Institute of Molecular Biology and Biotechnology, Foundation for Research and Technology – Hellas, Heraklion 70013, Greece

Abstract—Articular cartilage function relies on its unique mechanical behavior. Cartilage mechanics have been described by several analytic models, whose parameters are usually estimated by fitting their constitutive equations to stress-relaxation data. This procedure can be long and is prone to experimental and fitting errors. This study describes a novel methodology for estimating the biomechanical properties of cartilage samples based on their linearized frequency response, derived by applying a series of small-amplitude harmonic displacements superimposed to a bias strain. The proposed methodology, denoted as linearized frequency-domain method (LFM), was demonstrated by quantifying the effects of collagenase and hyaluronidase on cartilage, where it provided robust cartilage parameter estimates that overall agreed well with estimates obtained by stress-relaxation analysis. LFM was also applied to unveil the strain-dependent nature of porcine cartilage biomechanical parameters. Results showed that increasing the bias strain from 5% to 15% caused a significant decrease in cartilage permeability but did not have significant effect on the compression modulus and the Poisson's ratio. Apart from cartilage, LFM can potentially quantify the strain-dependent nature of tissues and biomaterials, thereby enhance tissue-level understanding on organ physiology and pathology, lead to better computational tissue models, and guide tissue engineering research.

Keywords—Viscoelasticity, Biomechanics, Frequency response, Extracellular matrix, Cartilage.

INTRODUCTION

Articular cartilage is a specialized connective tissue that covers the ends of joints, bears significant loads, and provides the lubricated surfaces required for articulation. Its function relies on its unique mechanical behavior that originates from its dense extracellular matrix (ECM), which consists mainly of collagen II fibers and proteoglycans.[20,32] Imposed mechanical loads and interactions with neighboring tissues expose chondrocytes to a diverse set of chemical, biological, and mechanical stimuli that regulate their metabolism, behavior, and gene expression.[9,26] Chondrocyte response can be classified as anabolic (ECM synthesis) or catabolic (ECM degradation). Normally, chondrocytes maintain cartilage ECM homeostasis by a dynamic equilibrium of anabolism and catabolism. However, in several pathological conditions this equilibrium is disrupted in favor of catabolism.[9] For example, in osteoarthritis decreased aggrecan expression and abnormal collagen expression lead to a vicious cycle of altered cartilage ECM, altered mechanical properties, altered mechanical stimuli to chondrocytes, and further catabolic shift of chondrocytes.[10,19]

Several models attempted to describe the complex mechanics of cartilage in physiology and pathology. The original biphasic model for confined and unconfined compression assumed that cartilage consists of a linear elastic solid phase and an incompressible non-dissipative fluid phase, where energy dissipation was attributed to friction at their interface.[1,21] The biphasic model has been evaluated and utilized extensively,[3,29] and has been extended in several ways. The biphasic poroviscoelastic (BPVE) model incorporated the intrinsic viscoelasticity of the solid matrix to the biphasic model.[18] The hyperelastic biphasic model

addressed the assumption of isotropic solid matrix.[2] The transversely isotropic biphasic (TIB) model considered tension–compression nonlinearity.[4,5] The biphasic Conewise Linear Elasticity (CLE) model considered tension–compression nonlinearity in the solid phase by employing the Conewise Linear Elasticity theory.[6,30] The biphasic-CLE-QLV (Quasi-Linear Viscoelastic) model added the viscoelasticity of the solid phase.[8,11,30] Finally, the triphasic model added an ion phase that considered the role of charged proteoglycans.[15] The Generalized Maxwell model is an alternative way to model cartilage viscoelasticity using combinations of springs and dashpots. Its simplest version, the Standard Linear Solid (SLS) model, consists of a spring parallel to a Maxwell element.

Cartilage mechanical properties are studied experimentally by several mechanical testing methods of *ex vivo* samples including unconfined compression, confined compression, and indentation. Based on the temporal profile of the applied load, experimental methods can be classified as time-domain (stress-relaxation, creep) or frequency-domain. Estimation of cartilage properties based on time-domain methods has been widely applied, yet this approach suffers from several limitations: first, a considerable amount of time is required for a cartilage sample to reach equilibrium due to its low fluid permeability. Second, fitting the multi-exponential constitutive equations of analytical models to stress-relaxation data is sensitive to noise and implementation. On the other hand, frequency-domain methods quantify cartilage response to harmonic compressive loads.[22,25,34] Although cartilage response to harmonic loads has been reported by several studies, to the best of our knowledge no prior study has suggested a way to analyze such data in order to get insight on cartilage biomechanical properties.

This study describes a novel linearized frequency-domain methodology (LFM) that exploits recent advances in instrumentation to analyze the response of cartilage samples to small-amplitude harmonic excitations and eventually provide robust estimates of cartilage biomechanical parameters. LFM was evaluated by quantifying the effects of two digestion enzymes on porcine cartilage, a simple model for cartilage degeneration that mimics disease state. This study demonstrated that LFM provided cartilage parameter estimates that generally agree with estimates obtained by the established method of analyzing stress-relaxation data. LFM was also utilized to quantify the strain-dependent nature of permeability in porcine cartilage. Applications of LFM are not limited to cartilage but can be extended to several areas of soft tissue biomechanics, biomaterials, and tissue engineering where the complex biomechanical behavior of samples needs to be analyzed.

MATERIALS AND METHODS

This section describes the experimental setup (instrument, enzymatic treatments, mechanical loading), the analytic models of cartilage viscoelasticity considered, and data analysis. Further details are provided in the supplementary material. Examples of MATLAB code that implements LFM are available at https://github.com/biolabntua/LFM.

Methodology Outline

The methodology consisted of three steps, Fig. 1a. First, a series of small-amplitude harmonic displacement profiles of increasing angular frequency ω_i superimposed to a bias strain were applied to a cartilage sample. Second, the acquired data were processed to calculate the frequency response function $H(j\omega_i)$, and a transfer function $H(s)$ was fitted to $H(j\omega_i)$. Third, cartilage material parameters were estimated based on analytic expressions of $H(s)$ derived from published cartilage models.

Experimental Methods

Instrumentation Description

Cartilage sample testing took place in an ElectroForce 3100 instrument (Bose, Framingham MA) running WinTest 4.0 software, equipped with a high-resolution force transducer (2.5 N max force, 1 mN resolution) and a LVDT position sensor (1 μm resolution). The instrument ran in closed loop position control configuration that provided 1.5 μm controllable peak-to-peak displacement.

Cartilage Sample Preparation

Joints from a 6-month-old healthy porcine were received from a local abattoir. Upon arrival, articular cartilage surfaces were exposed and rinsed with phosphate buffered saline (PBS). Thin slices of cartilage were harvested from lateral and medial condyle without subchondral bone, and were incubated for 24 h in a humidified incubator (37 °C, 5% CO_2) in PBS supplemented with penicillin and streptomycin (PBS + P/S). Cartilage disk samples (approximately 1.4 mm thick, Table S1) were cut using a $r = 3$ mm diameter biopsy punch. Consistent sample preparation is crucial for studies of cartilage biomechanics.[27] In the proposed methodology, firm and homogenous contact of indenter faces with cartilage sample faces was required
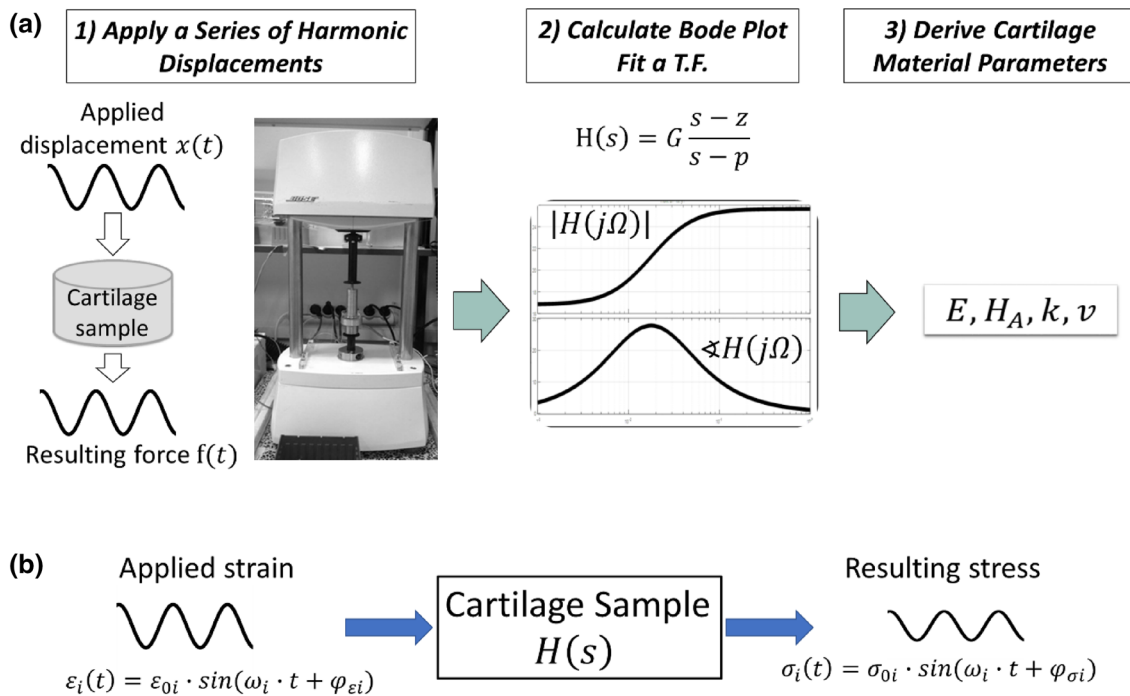
FIGURE 1. Outline of the proposed methodology (LFM) for quantifying cartilage viscoelasticity. (a) The methodology consists of three steps: (1) Apply a series of small-amplitude harmonic loads of increasing angular frequency superimposed to a bias strain. (2) Calculate the experimentally derived Bode plot and fit a simple transfer function. (3) Estimate cartilage material parameters based on published cartilage models converted in the frequency domain. (b) The viscoelastic behavior of a cartilage sample is modeled as a linear system described by a transfer function $H(s)$ that describes the input–output relationship between applied strain $\varepsilon(t)$ and the resulting engineering stress $\sigma(t)$.

during sample mechanical loading. In order to overcome the limitations of manual sample preparation, a custom instrument was designed to cut the bottom face of cartilage disk samples (remove material from the deep zone without affecting the superficial zone) in order to generate samples of consistent thickness and improved surface parallelism.

The height of each sample was measured using the ElectroForce press. The indenter was slowly lowered until a small load of 0.1 N registered the position x_1 of press bottom surface. Then, the indenter returned to its initial position and the cartilage specimen was placed on the press so that its surfaces were parallel to the plate surface. The indenter was slowly lowered again until a load measurement of 0.3 N registered the position x_2 of the sample top surface. The height of each cartilage specimen was calculated as $h = x_1 - x_2$. Samples were then stored at −80 °C until use.

Enzymatic Treatment

Samples were thawed in a 37 °C water bath following published guidelines,[33] transferred in a sterile 35 mm petri dish, and immersed in 0.5 mL solution: either PBS + P/S (control group), or 20 U/mL (0.1 mg/ml) type II collagenase (MP Biomedicals) in PBS + P/S, or 20 U/mL (0.035 mg/ml) hyaluronidase

grade I (Applichem) in PBS + P/S following previous protocols.[12,23] All groups contained $n = 6$ samples. After 24 h of incubation (37 °C, 5% CO_2), each sample was rinsed twice with PBS + P/S. Before mechanical testing, the thickness of each sample was measured again to identify enzyme-induced dimension alterations. No statistically significant difference in sample height was identified in all three groups, Table S1.

Sample Loading Protocol

Each cartilage sample was carefully positioned so that its bottom surface (bone side) made firm contact with the dish surface. The sample top surface (cartilage surface) faced the indenter. Initially, the press indenter moved slowly towards the sample until a load of 0.3 N indicated contact with the sample top surface. Then, a ramp displacement was applied to compress the specimen to the desired bias strain (5, 10 or 15%) at a rate of 0.05%/sec, and the specimen was equilibrated for 30 min. Then, a series of sinusoidal strains of 0.5% amplitude were superimposed to the bias strain at eight different frequencies for a defined number of cycles, Table 1 and Fig. 3a. The duration of the loading profile was 2 h and 40 min. During loading the indenter made firm contact with the top surface of the sample. The

position of the indenter and the force applied to the sample were sampled at 70 kHz.

Analytic Modeling of Cartilage Viscoelasticity

Three models were used to describe cartilage viscoelasticity: two analytic models of cartilage (the biphasic model[1] and the transversely isotropic biphasic (TIB) model[5]), and the SLS model. The biphasic model was chosen due to its widespread use. The TIB model was chosen because it is reported to model cartilage much better than the biphasic model, and because of its tractable analytic complexity. The SLS model was utilized as a generic way to model a viscoelastic material. Table 2 provides analytic expressions for the response of the mean stress $\sigma(t)$ to an unit ramp strain $\varepsilon(t)$. The expressions for the biphasic and TIB models were derived by considering only the first order of the analytic response. Table 2 also provides the corresponding transfer function $H(s) = \frac{\sigma(s)}{\varepsilon(s)}$ that describes the input–output relationship of a cartilage sample treated as a system whose input is the applied strain $\varepsilon(t)$ and whose output is the resulting stress response $\sigma(t)$, Fig. 1b.

Analysis of Frequency-Domain Data

Derivation of Experimental Frequency Response Function

The ith harmonic component $\varepsilon_i(t)$ of the applied strain $\varepsilon(t) = x(t)/h$ can be described as:

$$\varepsilon_i(t) = \varepsilon_{0i}\sin(\omega_i t + \varphi_{\varepsilon i})$$

where ω_i is the angular frequency of the ith harmonic, Fig. 1b. The resulting mean stress profile $\sigma(t) = F(t)/$

(πr^2) consisted of the homogenous and the specific response, Fig. 2b. The specific response included sinusoidal components $\sigma_i(t)$ response to $\varepsilon_i(t)$.

$$\sigma_i(T) = \sigma_{0i}\sin(\omega_i t + \varphi_{\sigma i})$$

For each one of the eight applied frequencies ω_i, $\sigma_i(t)$ was extracted from $\sigma(t)$ *via* digital filtering. The parameters ε_{0i}, $\varphi_{\varepsilon i}$, σ_{0i} and $\varphi_{\sigma i}$ were calculated by fitting a sinusoidal function to $\varepsilon_i(t)$ and $\sigma_i(t)$. Then, the complex frequency response function $H(j\omega_i)$ was obtained by calculating its magnitude $M_i = \frac{\sigma_{0i}}{\varepsilon_{0i}}$ and phase $\vartheta_i = \varphi_{\sigma i} - \varphi_{\varepsilon i}$. $H(j\omega)$ was visualized *via* a Bode plot, which consists of a plot of $20 \log_{10}(M_i)$ (in units of dB) and a plot of ϑ_i, both plotted as a function of $\log_{10}(\omega)$. The eight pairs (M_i, ϑ_i) comprised $H(j\omega_i)$, a discrete sampling of the system's $H(j\omega)$ at ω_i.

Transfer Function Fit to the Frequency Response Function

The following single-pole single-zero transfer function was then fitted to the pairs (M_i, ϑ_i):

$$H(s) = \frac{\sigma(s)}{\varepsilon(s)} = K\frac{s - z}{s - p}$$

where K, z, and p are the gain, zero and pole of $H(s)$. This simple transfer function can describe various cartilage models, including the SLS model, the biphasic model of order one, and the TIB model of order one. The values $\hat{x}_h = \begin{bmatrix} \hat{K} & \hat{z} & \hat{p} \end{bmatrix}^T$ of $H(s)$ parameters $x_h = [K, z, p]^T$ that fitted $H(j\omega_i)$ were calculated by nonlinear least-squares implemented in MATLAB (Mathworks, Natick MA) that minimized the mean squared error (MSE) $MSE_f(x_h)$ metric, where $MSE_f(x)$ was defined as:

TABLE 1. Frequencies and number of cycles for the applied harmonic displacement profile.

Frequency (Hz)	0.002	0.005	0.009	0.02	0.04	0.1	0.5	1
Angular frequency (rad/s)	0.0126	0.0314	0.0565	0.125	0.251	0.628	3.14	6.28
Number of cycles	5	5	10	10	25	40	210	420

TABLE 2. Analytic relations that describe cartilage response in time and frequency domains based on three published models.

Model	Response $\sigma(t)$ to a unit ramp strain $\varepsilon(t)$	Transfer function $H(s) = \frac{\hat{\sigma}(s)}{\hat{\varepsilon}(s)} = K(s - z)(s - p)^{-1}$
SLS	$E_0\left\{t + \frac{\eta_1}{E_0}\left(1 - e^{-\frac{E_1}{\eta_1}t}\right)\right\}$	$(E_0 + E_1)(s + \frac{E_0 E_1}{\eta_1(E_0 + E_1)})(s + \frac{E_1}{\eta_1})^{-1}$
Biphasic	$E_S\left\{t + \frac{a^2}{H_A k}\left[\frac{1}{8}\frac{(1-v)(1-2v)}{(1+v)} - \frac{A_1}{a_1^2}e^{-\frac{a_1^2 H_A k t}{a^2}}\right]\right\}$	$E_S(1 + A_1)(s + \frac{a_1^2 H_A k}{a^2(1+A_1)})(s + \frac{a_1^2 H_A k}{a^2})^{-1}$
TIB	$E_3\left\{t + \frac{E_1}{E_3}\frac{a^2}{C_{11}k}\Delta_3\left\{\frac{1}{8} - \frac{1}{a_1^2\left(\Delta_2^2 a_1^2 - \frac{\Delta_1}{(1+v_{21})}\right)}e^{-\frac{a_1^2 C_{11}k t}{a^2}}\right\}\right\}$	$E_3(1 + c_1)(s + \frac{a_1^2 C_{11}k}{a^2(1+c_1)})(s + \frac{a_1^2 C_{11}k}{a^2})^{-1}$

For each model, the transfer function $H(s)$ that describes cartilage viscoelasticity (right column) is derived from published analytic expressions of stress response $\sigma(t)$ of cartilage to a step displacement stimulation.
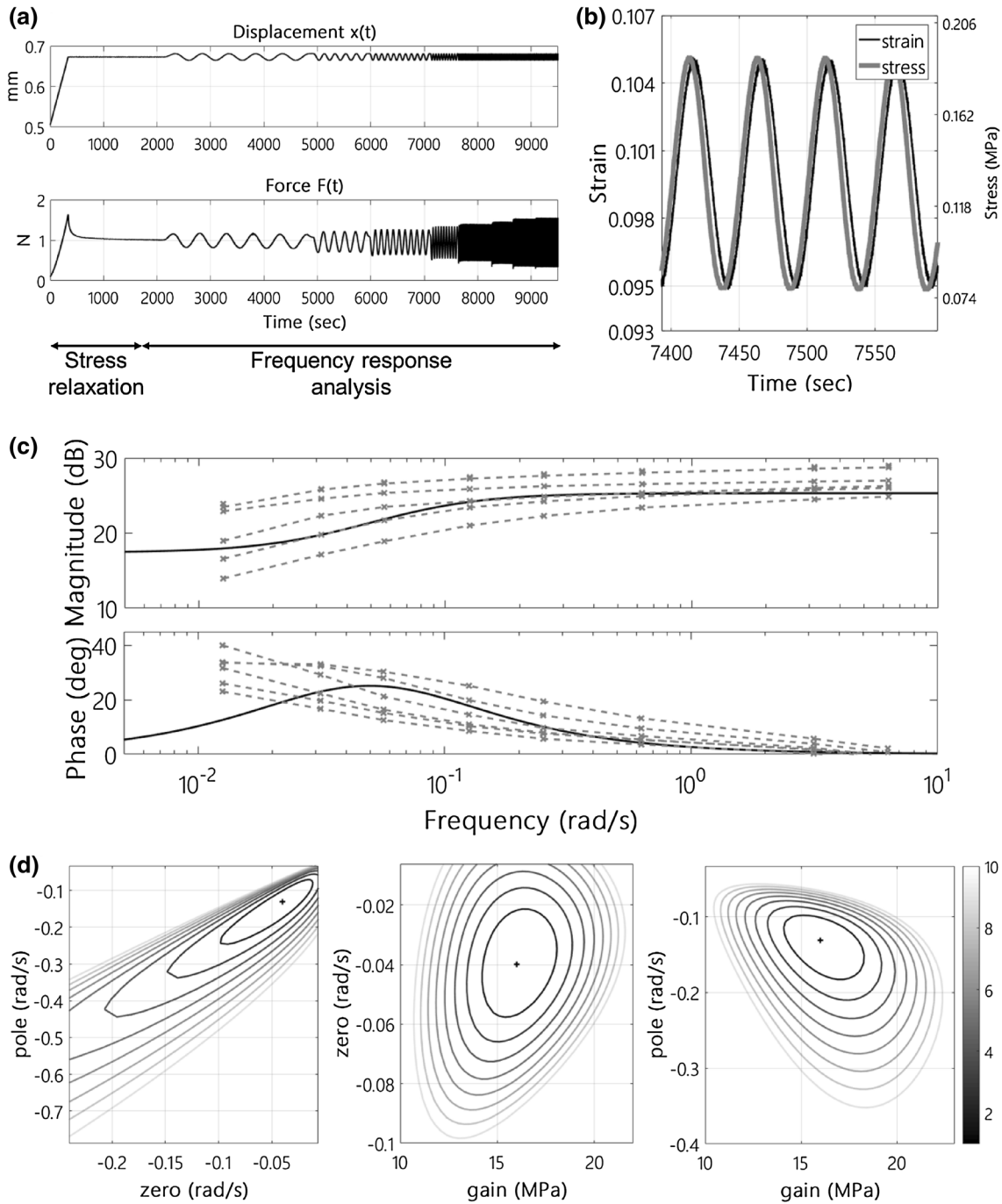
FIGURE 2. Experimental derivation of the frequency response function $H(j\omega_i)$ and the corresponding transfer function $H(s)$ that best describes the linearized viscoelastic behavior of control porcine cartilage samples. (a) Representative time profiles of the displacement profile applied to cartilage tissue samples, and the resulting measured force. The final bias displacement corresponds to a 10% strain, while superimposed harmonics correspond to 0.5% strain amplitude around the bias. The plot highlights the parts of the response used for the frequency response analysis and for stress-relaxation analysis. (b) Zoom in one of the harmonics of image A highlights the phase difference between them due to cartilage viscoelasticity. (c) Bode plot of the mean transfer function $H(s)$ superimposed to experimental sampling of $H(j\omega_i)$ ('x') from $n = 6$ control cartilage samples. (d) Sensitivity analysis for the estimation of $H(s)$ parameters (gain, zero, pole) for a representative cartilage sample. Contour plots of the normalized fitting error $MSE_f(x_h)/MSE_f(\hat{x}_h)$ in the proximity of estimated $H(s)$ parameter values $\hat{x}_h$, which are denoted with a "+".

$$MSE_f(\boldsymbol{x}) = \frac{1}{N_h} \sum_{i=1}^{N_h} (H(j\omega_i) - \hat{H}(j\omega_i, \boldsymbol{x}))^2$$

where N_h is the number of frequencies, $H(j\omega)$ is experimentally sampled, $H(j\omega_i) = M_i \cdot e^{j \cdot \vartheta_i}$ is the experimentally-derived frequency response function,

and $\hat{H}(j\omega_i, \boldsymbol{x}) = \hat{M}_i(\boldsymbol{x}) \cdot e^{j \cdot \hat{\vartheta}_i(\boldsymbol{x})}$ is the analytic expression of $H(j\omega)$ predicted by the model given parameters $\boldsymbol{x}$. The robustness of $\hat{\boldsymbol{x}}_h$ estimates was evaluated by calculating $\text{MSE}_f(\boldsymbol{x}_h)$ in the 3-dimensional space $\boldsymbol{x}_h$ around $\hat{\boldsymbol{x}}_h$.

Estimation of Cartilage Material Parameters

Based on $H(s)$ parameters, $\hat{\boldsymbol{x}}_h$, cartilage material properties were estimated for each model by utilizing the corresponding analytic expressions of $H(s)$ shown in Table 2. The SLS model and the biphasic model contain 3 parameters each, which were calculated directly from $\hat{\boldsymbol{x}}_h$. The TIB model contains five parameters (E_1, E_3, v_{21}, v_{31}, k), where only E_3 could be calculated directly from $\hat{\boldsymbol{x}}_h$. The remaining parameters were derived as functions of ratios $e = E_1/E_3$ and $n = v_{21}/v_{31}$, after solving the following equation for v_{21}:

$$c_1(v_{21}, e, n) = \frac{\hat{p}}{\hat{z}} - 1 \qquad (1)$$

This equation provides meaningful solutions ($0 \leq v_{21} \leq 0.5$) when ratios e, n take values within a data-dependent region ($\hat{z}$, $\hat{p}$ were derived from experimental data). Therefore, the remaining parameters of the TIB model were calculated assuming reasonable values of ratios e and n within the region of meaningful solutions. The robustness of TIB model parameter estimates $\hat{\boldsymbol{x}}_{\text{TIB}}$ was evaluated by calculating the $\text{MSE}_f(\boldsymbol{x}_{\text{TIB}})$ metric in the proximity of $\hat{\boldsymbol{x}}_{\text{TIB}}$.

Analysis of Stress-Relaxation Data

The stress response $\sigma(t)$ to the ramp strain displacement applied to cartilage samples in the beginning of the loading profile (before the onset of harmonic loads, Fig. 2a) was utilized to estimate cartilage parameters by the standard method of fitting analytic models to stress-relaxation data. Analytical expressions of stress response, Table S1, were fitted to $\sigma(t)$ measurement in MATLAB using either nonlinear least-squares (fitting the SLS model) or interior-point constrained nonlinear optimization (fitting the biphasic or TIB models). Cartilage material parameter estimates $\hat{\boldsymbol{x}}$ minimized the following $\text{MSE}_t(\boldsymbol{x})$ metric:

$$\text{MSE}_t(\boldsymbol{x}) = \frac{1}{N_t} \sum_{i=1}^{N_t} (\sigma(t_i) - \hat{\sigma}(t_i; \boldsymbol{x}))^2$$

where $\boldsymbol{x}$ is the parameter vector of each model, $\sigma(t_i)$ is the measured stress at time point t_i, N_t is the number of time points, and $\hat{\sigma}(t_i; \boldsymbol{x})$ is the analytic expression of the stress response predicted by the model given parameter vector $\boldsymbol{x}$. The robustness of the resulting estimates $\hat{\boldsymbol{x}}$ was evaluated by calculating $\text{MSE}_t(\boldsymbol{x})$ in the parameter space around $\hat{\boldsymbol{x}}$.

Statistical Analysis

Experimental data and estimated parameters presented are expressed as mean $\pm$ standard error of the mean. Statistical significance of parameter differences of enzyme-treated sample groups compared to the untreated group was assessed by pair-wise two-sided t tests. Statistical significance of the effect of bias strain on TIB model estimates was assessed by single-factor ANOVA.

RESULTS

Estimation of Cartilage Material Parameters from the Linearized Frequency Response

Figure 2a shows representative experimental results (applied displacement $x(t)$, resulting force $F(t)$) of unconfined compression experiments in control porcine cartilage samples. The resulting force $F(t)$ lagged the applied displacement $x(t)$, Fig. 2b, in a frequency-dependent way. A closer look on $x(t)$ and $F(t)$ demonstrated the smoothness of measured data, Fig. S3. The experimentally derived $H(j\omega_i)$ at each ω_i was calculated based on the magnitude and phase of the harmonic components $\varepsilon_i(t)$, $\sigma_i(t)$ of strain and stress respectively, shown in Fig. 2c.

The validity of the linearization assumption was evaluated by applying sinusoidal strains of increasing amplitude (0.5, 1, 3%) and deriving $H(j\omega_i)$. The $H(j\omega_i)$ obtained by harmonic strain amplitudes of 0.5 and 1% were indistinguishable, Fig. S5, in agreement with the key property of linear systems that $H(j\omega)$ is independent of excitation amplitude.

Based on $H(j\omega_i)$, the optimal parameters $\hat{\boldsymbol{x}}_h = \begin{bmatrix} \hat{K} & \hat{z} & \hat{p} \end{bmatrix}^T$ of a single-zero single-pole transfer function $H(s)$ were identified by fitting to $H(j\omega_i)$ for each sample. Preliminary calculations suggested that such a simple $H(s)$ can approximate well the frequency response function $H(j\omega)$ of cartilage samples since the responses of biphasic and the TIB models are dominated by their first order, Fig. S11. The average of $\hat{\boldsymbol{x}}_h$ parameters from 6 cartilage samples, Table 3, were utilized as the parameters of a mean transfer function $\bar{H}(s)$ that described the viscoelasticity of the control porcine cartilage group. The Bode plot of $\bar{H}(s)$, Fig. 2c, matched well the magnitude and showed reasonable agreement with the phase of measured $H(j\omega_i)$, although the phase peak at $\omega = 0.055$ rad/s was not clear in $H(j\omega_i)$. The shape of fitting error MSE_f suggested that $\hat{\boldsymbol{x}}_h$ were estimated robustly (MSE_f increases rapidly away from $\hat{\boldsymbol{x}}_h$) in the K–z and K–p planes, Fig. 2d. The shape of MSE_f on the z–p plane suggested that the ratio $\hat{p}/\hat{z}$ was estimated with higher confidence compared to the values of $\hat{p}$ and $\hat{z}$, Fig. 2d and Table 3.

Finally, cartilage material parameters were estimated from the parameters $\hat{x}_h$ of $H(s)$ by utilizing the analytic expressions for $H(s)$ shown in Table 2. The resulting parameter estimates are shown in Tables 4 and S3. SLS model parameters were directly calculated from $\hat{x}_h$ as $E_0 = 7.82 \pm 1.22$ MPa, $E_1 = 13.19 \pm 0.81$ MPa, and $\eta_1 = 321 \pm 97$ MPa · s. The parameters of the biphasic model were also directly calculated as $E_s = 7.82 \pm 1.22$ MPa, $v = 0 \pm 0$, and $k = 6.33 \pm 2.6 \times 10^{-15}$ m^4/N · s. The locus of e, n where the TIB model provided meaningful estimates for the average control porcine cartilage sample is shown in Fig. 3b. Plots of $c_1(v_{21}, e, n)$ suggest that e had stronger effect compared to ratio n, Fig. 3a. The locus shown in Fig. 3b indicates that ratio e is upper bounded, e.g., assuming $n \approx 1$ ($v_{21} \approx v_{31}$, a commonly used assumption) then $E_1/E_3 < 4.49$. Assuming $e = 2.22$ and $n = 1$ (chosen so $v_{21} = v_{31} \approx 0.25$, the mean of published results, Fig. S11) TIB model parameters were estimated as $E_3 = 7.82 \pm 1.22$ MPa, $E_1 = 17.36 \pm 2.71$ MPa, $v_{21} = 0.25 \pm 0.03$, and $k = 1.05 \pm 0.33 \times 10^{-15}$ m^4/N · s. The assumed values of e, n affected more v_{21}, v_{31}, E_1 estimation and less k estimation, Table S3. Finally, the normalized MSE$_f$ in the E_3–v_{21}–k space increases rapidly away from estimated values, suggesting robust estimation of TIB model parameters, Fig. 3c.

Estimation of Cartilage Material Properties from Stress-Relaxation Experiments

Cartilage parameter estimates obtained by LFM were compared against estimates obtained by analyzing stress-relaxation data. Figure 4a shows the resulting fits of the analytic stress expressions predicted by the biphasic and the TIB models, Table S2, to the stress response $\sigma(t)$ of porcine cartilage samples, Fig. 2a. Both models fitted well the equilibrium response and fitted poorly the transient peak stress. Fitting the biphasic model provided $E_S = 1.98 \pm 0.47$ MPa, $v = 0 \pm 0$ and $k = 1.15 \pm 0.21 \times 10^{-15}$ m^4/N · s. Fitting the TIB model provided $E_1 = 5.93 \pm 1.26$ MPa, $E_3 = 1.89 \pm 0.47$ MPa, $v_{21} \approx v_{31} = 0.08 \pm 0.02$, and $k = 0.7 \pm 0.17 \times 10^{-15}$ m^4/N · s. The shallow non-steep shape of the fitting error MSE$_t$ around parameter estimates was an indication of poor estimation robustness, particularly for Poisson's ratio v estimates, Fig. 4b.

Effect of Enzyme Digestion on Linearized Cartilage Frequency Response

The effect of collagenase and hyaluronidase treatment on cartilage viscoelasticity was quantified by the proposed LFM and by stress-relaxation analysis. Fig-

TABLE 3. Statistics of the three parameters (gain, zero, pole) of the transfer function that describe the viscoelasticity of the three cartilage groups considered in this study, as well as the resulting pole/zero ratio.

	Control	Collagenase	Hyaluronidase
Gain $\hat{K}$	21.02 ± 1.64	7.85 ± 1.58***	19.40 ± 3.07
Pole $\hat{p}$	-0.057 ± 0.017	-0.196 ± 0.047**	-0.214 ± 0.085
Zero $\hat{z}$	-0.019 ± 0.004	-0.011 ± 0.003	-0.074 ± 0.03
$\hat{p}/\hat{z}$ ratio	2.88 ± 0.26	19.4 ± 2.68***	2.91 ± 0.26

Results are expressed as mean $\pm$ SEM. Statistically significance of parameter estimate differences of enzyme-treated samples compared to control samples was determined by a t test: * $p < 0.1$; ** $p < 0.05$; *** $p < 0.01$.

TABLE 4. Estimated cartilage material parameters for the three cartilage sample groups (control, collagenase-treated, hyaluronidase-treated) estimated by LFM or by the established stress-relaxation method based on the biphasic model and the TIB model.

Method	Parameter	Control	Collagenase	Hyaluronidase
Frequency domain	E_3 (MPa)	7.82 ± 1.22	0.51 ± 0.19***	7.09 ± 1.51
	E_1 (MPa)	17.36 ± 2.71	1.13 ± 0.42***	15.74 ± 3.34
	v_{21}	0.25 ± 0.034	0.37 ± 0.001**	0.26 ± 0.02
	v_{31}	0.25 ± 0.034	0.37 ± 0.001**	0.26 ± 0.02
	k (10^{-15} m^4/N · s)	1.05 ± 0.33	6.01 ± 1.33**	5.98 ± 3.16
Stress relaxation	E_3 (MPa)	1.89 ± 0.47	0.14 ± 0.06**	0.89 ± 0.25*
	E_1 (MPa)	5.93 ± 1.26	1.16 ± 0.52**	4.95 ± 0.85
	v_{21}	0.08 ± 0.02	0.21 ± 0.01***	0.05 ± 0.01
	v_{31}	0.08 ± 0.02	0.19 ± 0.03**	0.05 ± 0.01
	k (10^{-15} m^4/N · s)	0.70 ± 0.17	7.17 ± 0.92***	0.68 ± 0.11

Results are expressed as mean $\pm$ SEM. Statistically significance of parameter estimate differences of enzyme-treated samples compared to control samples was determined by a two-tail t test: * $p < 0.1$; ** $p < 0.05$; *** $p < 0.01$.
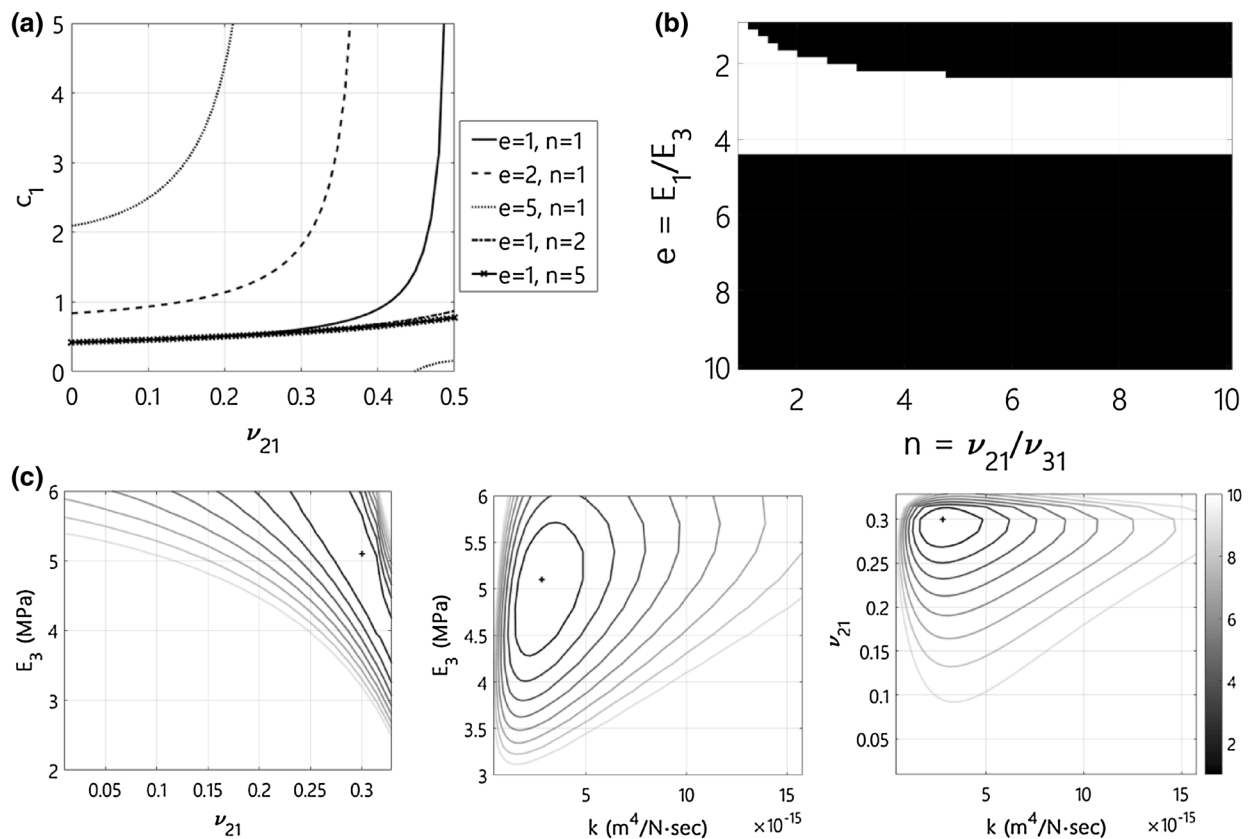
FIGURE 3. Estimation of TIB model parameters by interpreting the parameters of the transfer function $H(s)$ that fits the experimentally-derived frequency response function $H(j\omega_i)$ of control cartilage samples. (a) Plots highlighting the effect of ratios $e = E_1/E_3$ and $n = v_{21}/v_{31}$ in the function $c_1(v_{21})$. (b) The region of ratios e and n where the function $c_1(v_{21}) = \frac{p}{z} - 1$ has meaningful solution. (c) Sensitivity analysis for the estimation of TIB model cartilage material parameters for a representative cartilage sample assuming $e = 2.22$, $n = 1$. Contour plots of the normalized fitting error $MSE_f(x_{TIB})/MSE_f(\hat{x}_{TIB})$ in the proximity of estimated model parameter values $\hat{x}_{TIB}$, denoted with a "+".

ure 5a shows the experimentally-derived $H(j\omega_i)$ for the three sample groups. Collagenase treatment reduced significantly the magnitude $|H(j\omega_i)|$, increased significantly phase $\angle H(j\omega_i)$, and shifted the peak of $\angle H(j\omega_i)$ towards larger ω. The mean $|H(j\omega_i)|$ of hyaluronidase-treated samples was less (but not significantly significant) compared to control samples. The resulting $H(s)$ parameter estimates for each sample group are shown in Table 3. Collagenase treatment decreased significantly the gain $\hat{K}$, shifted pole $\hat{p}$ towards faster response, but did not have a statistically significant effect on zero $\hat{z}$. Collagenase had also a significant effect on the $\hat{p}/\hat{z}$ ratio, a parameter that affects the estimation of Poisson's ratio. On the other hand, hyaluronidase treatment resulted in non-statistically significant increase in pole and zero magnitude.

Figure 5b shows representative stress-relaxation responses for the three sample groups. The stress response of collagenase-treated samples reached significantly less equilibrium stress, and displayed faster viscoelastic response. Rapid stress variations in the

beginning and the end of the strain ramp loading, Fig. S10, complicated model fitting since their magnitude (around 20 mN) was on the same order of magnitude as the force utilized to register indenter-sample contact. Hyaluronidase treatment resulted in significantly less equilibrium stress, despite the finding that $H(j\omega_i)$ of hyaluronidase-treated samples was not significantly distinct from the one of control samples, Fig. 5a.

Figures 5c–5e and Table 4 summarize the resulting estimates of TIB model parameters for the three sample groups. Regarding axial compressive modulus E_3, LFM suggested that only collagenase treatment caused statistically significant decrease in E_3. Stress-relaxation analysis provided smaller E_3 estimates than LFM, and suggested that both collagenase and hyaluronidase treatment caused statistically significant decrease in E_3, Fig. 5c. Regarding Poisson's ratio estimates, both methods suggested that only collagenase treatment caused statistically significant increase in v_{21}, Fig. 5d. Stress-relaxation analysis provided smaller v_{21} esti-
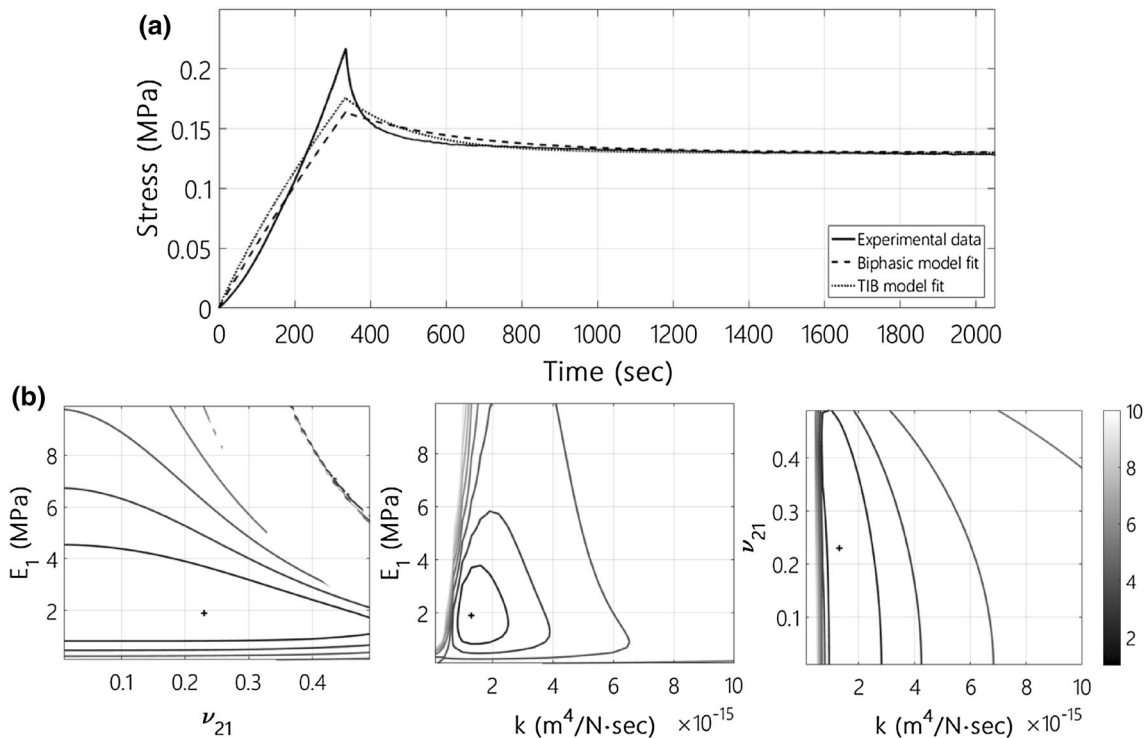
FIGURE 4. Estimation of cartilage parameters based on stress-relaxation data. (a) Representative results of estimating the parameters of the biphasic model and the TIB model by fitting them to experimental stress-relaxation data. (b) Representative sensitivity analysis plots for parameter estimates provided by fitting the TIB model to stress-relaxation data. Contour plots of the normalized fitting error $\text{MSE}_t(x)/\text{MSE}_t(\hat{x})$ in the proximity of estimated model parameter values $\hat{x}$, which are denoted with a "+".

mates compared to LFM. Finally, both methods suggested that collagenase but not hyaluronidase treatment caused statistically significant increase in tissue permeability k, Fig. 5e.

Table S3 also shows the resulting estimations of Biphasic model and SLS model parameters for the three sample groups. Estimation of Biphasic model parameters by both methods resulted in the trivial result $v = 0 \pm 0$ for all three groups. LFM provided larger estimates of E_S and k compared to stress-relaxation analysis. Both methods suggested that E_S is affected only by collagenase. Estimation of SLS model parameters by LFM provided larger estimates of E_0 and E_1 compared to stress-relaxation analysis. Finally, both methods suggested that E_0 and E_1 are reduced by collagenase, while E_0 is also reduced by hyaluronidase.

Effect of Strain Bias on Linearized Cartilage Frequency Response

In order to evaluate the effect of strain bias on the linearized frequency response of cartilage samples, LFM was applied to estimate the material parameters of control porcine samples pre-strained at 5% ($n = 5$), 10% ($n = 6$) or 15% ($n = 5$) bias before

applying the eight harmonic loads of Table 1. Results suggested that larger bias resulted in significant decrease in phase $\angle H(j\omega_i)$ and had less clear effect on magnitude $|H(j\omega_i)|$, Fig. 6a. Figures 6b–6d show the resulting estimates of TIB model parameters obtained at each bias strain. Results show that the bias strain did not have a statistically significant effect on E_3 ($p_{\text{anova}} = 0.19$) or v_{21} ($p_{\text{anova}} = 0.590$), but had a statistically significant effect on tissue permeability k ($p_{\text{anova}} = 0.023$) that decreases significantly at larger bias strains.

DISCUSSION

This paper describes a novel methodology for acquiring the linearized frequency response $H(j\omega)$ of cartilage samples in unconfined compression and interpreting it for estimating cartilage material parameters. The proposed LFM differs from previous frequency-domain studies of cartilage viscoelasticity in two ways. First, it utilizes analytic models of cartilage viscoelasticity to estimate cartilage material properties based on the experimentally-derived $H(j\omega)$. In contrast, previous studies that reported cartilage storage E' and
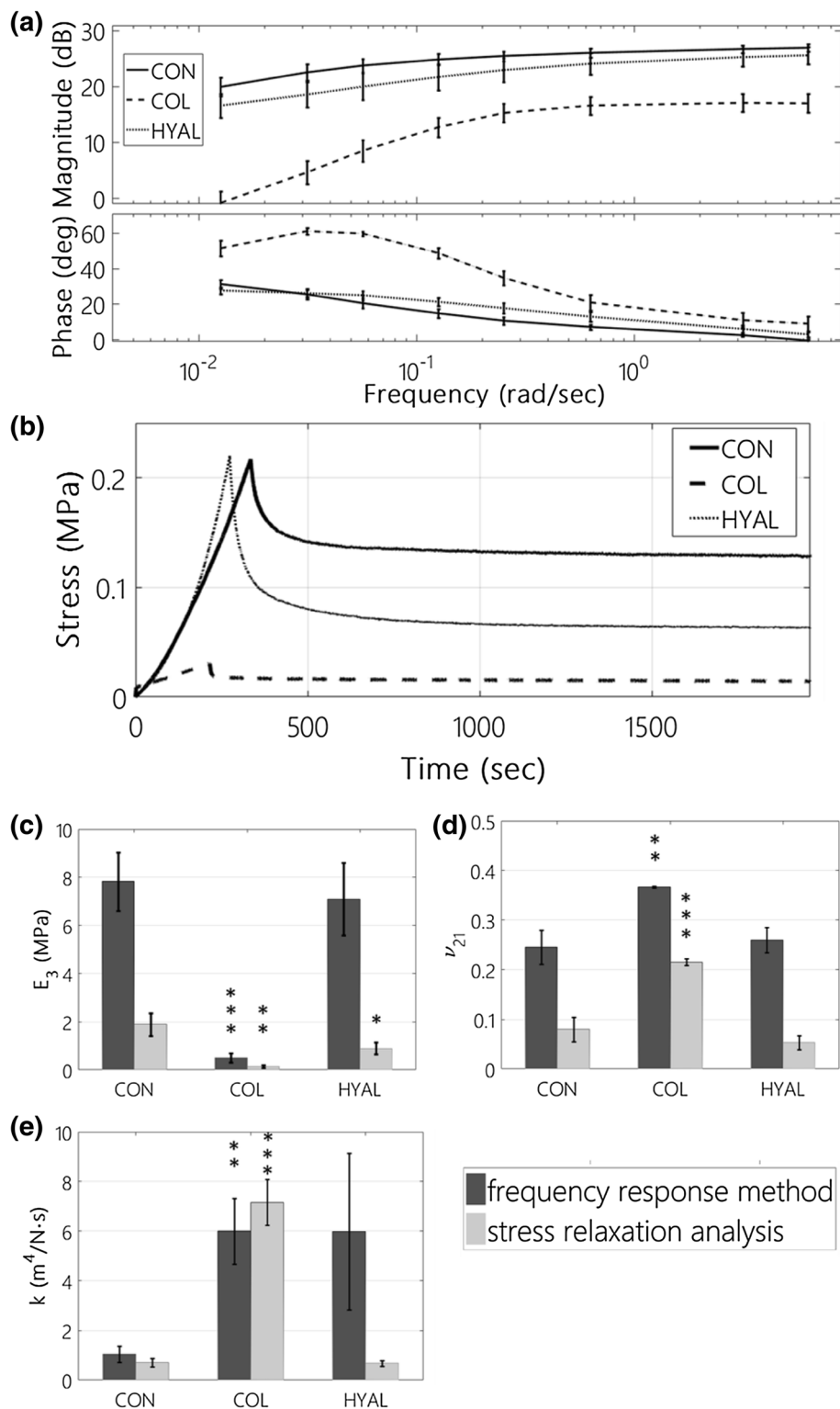
FIGURE 5. Effects of cartilage digestion enzymes on cartilage viscoelasticity as described by LFM and by stress-relaxation analysis. (a) Bode plots of the frequency response function $H(j\omega_i)$ as measured in control (CON), collagenase-treated (COL) and hyaluronidase-treated (HYAL) cartilage sample groups. (b) Representative stress-relaxation responses of the three sample groups (CON, COL, HYAL). (c–e) Estimates of TIB model parameters for the three sample groups provided by LFM (assuming $e = 2.22$, $n = 1$) and by stress-relaxation analysis. Data are presented as mean $\pm$ SEM. The statistical significance of differences in parameter estimates of enzyme-treated samples (COL, HYAL) compared to control CON samples was determined by a t test: $*p < 0.1$; $**p < 0.05$; $***p < 0.01$.
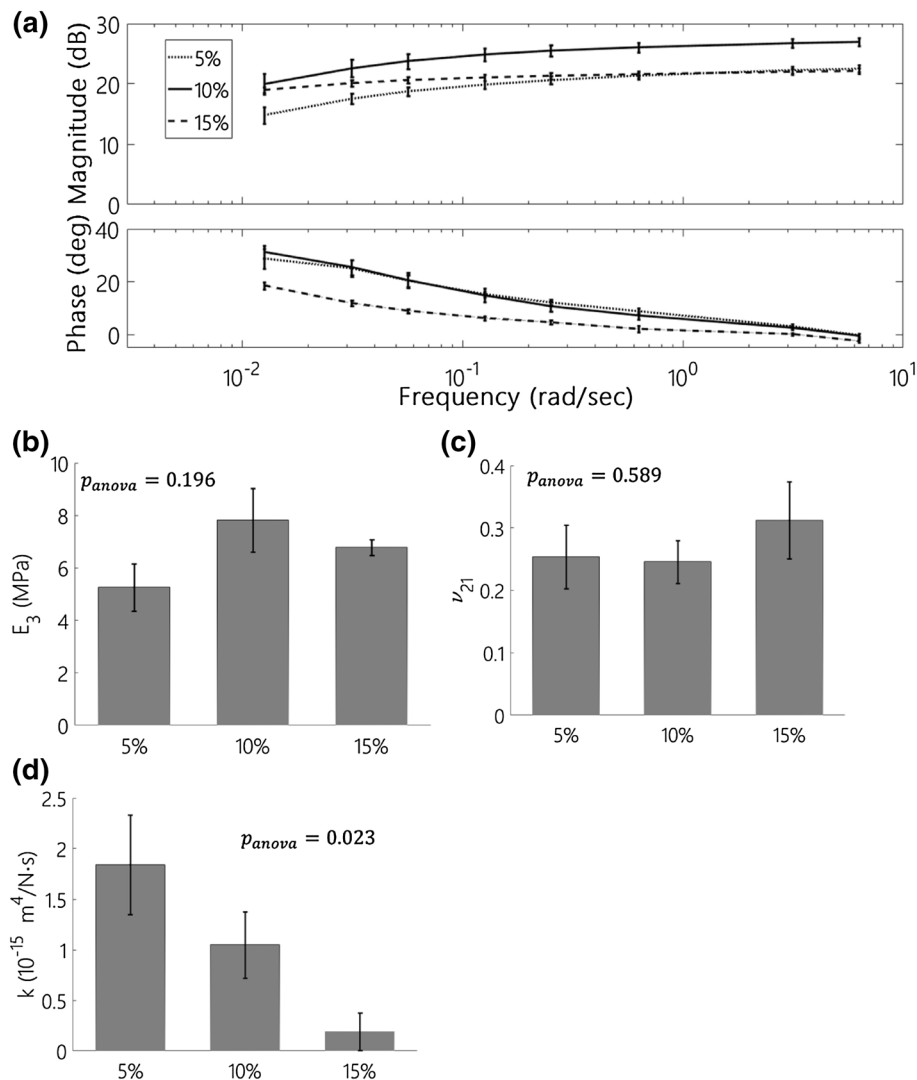
FIGURE 6. Effects of different bias strains on the frequency response of cartilage and on estimated cartilage material parameters. (a) Bode plots of the frequency response function $H(j\omega_i)$ obtained at bias strains of 5, 10, and 15%. (b–d) TIB model parameter estimates obtained by LFM at bias strains of 5, 10, and 15% (mean ± SEM).

loss modulus E'' (the real and imaginary part of $H(j\omega)$) did not proceed into analyzing their frequency dependence in order to estimate cartilage material parameters.[22,25,34] Second, LFM exploits the capabilities of state-of-the-art testing instrumentation to quantify the response of cartilage samples to small-amplitude harmonic strains (the instrument utilized here provided ≈ 1 μm position precision, and ≈ 1 mN force measurement resolution). Applying such small displacements ensures that the sample behaves like a linear system, which simplifies data analysis. In contrast, most previous studies applied larger strains (around $\pm 5\%$), where cartilage does not behave linearly, complicating data interpretation. The application of small harmonic strains over a larger bias strain, Fig. 2a, ensured that

samples made firm contact with press plates, and prevented artifacts due to sample lift off.

The frequency response function $H(j\omega_i)$ provided by LFM for control porcine cartilage samples, Fig. 2c, was in reasonable agreement with previous reports of cartilage response to harmonic loads (magnitude $|H(j\omega_i)|$ reached a plateau for $\omega > 1$ rad/s, phase $\angle H(j\omega_i)$ peaked at 35° around 0.02 rad/s).[22,23,25,31,34]

Estimation of cartilage material parameters from the experimentally-derived $H(j\omega_i)$ utilized Laplace-transformed constitutive equations of three analytic cartilage models. The established biphasic model performed poorly, in agreement with previous critique.[1,3] Interpreting $H(j\omega_i)$ using the biphasic model provided the trivial result $v = 0$ in all sample groups and bias

strains. Computational estimates of $H(j\omega)$ obtained by the biphasic model differed significantly from $H(j\omega_i)$ measurements, Fig. S11C. On the contrary, interpreting $H(j\omega_i)$ using the transversely isotropic biphasic (TIB) model resulted in cartilage parameter estimates that agreed well with previous estimates, Table 4.[3–5,21,29] Finally, interpreting $H(j\omega_i)$ via the SLS model was implemented as a generic way to model viscoelastic materials. Further analysis showed that the TIB model provided meaningful parameter estimates in porcine cartilage samples when tension–compression anisotropy ratios E_1/E_3 and v_{21}/v_{31} took values within a specific region, Fig. 3b, suggesting that cartilage is less anisotropic ($E_1/E_3 \leq 4.5$) than previously estimated ($E_1/E_3 \approx 10$).[5]

LFM sensitivity was initially evaluated by quantifying the effects of two degradation enzymes on cartilage material parameters. The effects of these enzymes emulate ECM degradation during cartilage pathology. Collagenase treatment had significant effects in $H(j\omega_i)$ measurements and the resulting $H(s)$ parameter estimates, Table 3. Interpreting $H(j\omega_i)$ via the TIB model suggested that collagenase treatment decreased the axial compression modulus E_3, and increased Poisson's ratios and tissue permeability k, Table 4. These effects agree with the role of collagen in cartilage ECM, where collagen fibrils provide tension stiffness and restrict proteoglycans (PG) that provide compression stiffness.[23,33] Degradation of collagen network can lead to reduced compression stiffness due to reduced PG constraint by the surrounding collagen network. The same rationale can also explain the increase in tissue permeability, since less constrained PG can move more easily. Previous studies have shown that collagen content and network integrity are inversely correlated to Poisson's ratio.[13,14] According to these studies, disruption of collagen network would result in a material that is more prone to swelling, since compressive modulus is decreased. This finding could explain the estimated increase in Poisson's ratio after collagenase digestion. On the other hand, the applied hyaluronidase treatment did not have strong effect on the measured $H(j\omega_i)$, and increased slightly (not statistically significant) the magnitude of $H(s)$ pole and zero. Interpreting $H(j\omega_i)$ via the TIB model suggested that hyaluronidase increased slightly (not statistically significant) tissue permeability k but did not have significant effects on other TIB model parameters, Table 4. Hyaluronic acid interconnects PG molecules, therefore its degradation should favor PG mobility and therefore could increase tissue permeability. A previous study that probed hyaluronidase effects to cartilage viscoelasticity reported decreased equilibrium modulus, and faster response.[12] Although LFM did not detect significant effects in equilibrium modulus,

the detected increase in permeability k corresponds to faster response since the system's time constants are inversely analogous to k. Finally, interpreting $H(j\omega_i)$ by the SLS model suggested that stiffness parameters E_0, E_1 were decreased only by collagenase, while the damping parameter η_1 was decreased by both collagenase and slightly (not statistically significant) by hyaluronidase, Table S3.

Since this study introduces LFM as a novel way to estimate cartilage parameter estimates, it was of interest to compare LFM estimates against the ones provided by the established stress-relaxation analysis. Overall, LFM provided similar trends but larger estimates of compression moduli and Poisson's ratios, and similar estimates of tissue permeability, Figs. 5c–5e.[4,5] Both methods suggested that collagenase treatment decreased E_3, and increased v_{21} and k, Fig. 5c–5e. Stress-relaxation analysis suggested that hyaluronidase treatment decreased E_3, Fig. 5c, while LFM suggested that hyaluronidase treatment had no effect on E_3 and caused a non-statistically significant increase in k. The difference in parameter estimates provided by the two methods may be attributed to the effect of linearization: LFM quantifies cartilage viscoelasticity within a narrow range of strain around the bias strain, while stress-relaxation experiments quantify cartilage viscoelasticity over a much larger range of strain values. For example, a stiffness parameter (e.g., E_3) quantified by LFM corresponds to the slope of the corresponding stress–strain curve at the bias strain, while the estimate of the same parameter obtained by stress-relaxation corresponds to some kind of "average" slope of the curve over the measured strain range.

A key feature of LFM is that by quantifying $H(j\omega_i)$ at different bias strains it is possible to estimate cartilage parameters at different strains, thereby uncover their strain-dependent nature. Very few reports of strain-dependent estimation of cartilage parameters by stress-relaxation analysis have been reported, possibly due to experimental limitations that induce estimation error (described in the following paragraph). Indeed, experimental results suggested that cartilage permeability k decreased at larger bias strains, Fig. 6d, in agreement with previous reports.[16] Decreased permeability at larger strains could originate from the increased resistance that fluid needs to overcome in order to flow through the more densely packed compressed matrix. Not all cartilage parameters were found to be strongly strain-dependent, as no significant effect of bias strain was observed on E_3 and v_{21}, Figs. 6b and 6c.

LFM offers several advantages compared to stress-relaxation analysis. First, linearizing cartilage viscoelasticity enables utilizing the available toolkit of linear systems analysis. Second, $H(j\omega_i)$ and $H(s)$

parameters can be used as descriptors of cartilage viscoelasticity in a model-independent way. Third, it provided more robust cartilage parameter estimates compared to stress-relaxation analysis (as judged by the shape of the fitting MSE in the proximity of parameter estimates, Figs. 3c and 4b) due to several favorable features: it avoids multi-exponential curve fitting to experimental data, it utilizes linear models to fit a linearized system, and it does not suffer from fitting errors caused by stress discontinuities (Fig. S10) or sensor drift (e.g., due to solvent evaporation, Fig. S4) sometimes present in stress-relaxation data. Finally, the application of small-magnitude harmonic displacements did not affect cartilage samples over at least 12 h, Fig. S5, enabling applying multiple harmonic load cycles over long periods and monitoring time-dependent phenomena.

The experimental implementation of LFM presented in this study can be improved in several ways. First, the duration of the applied loading profile was quite long (2 h 40 min) mostly due to the sequential application of several slow harmonic excitations (required for quantifying the information-rich region of $H(j\omega)$), Fig. 2c. The duration of the loading profile can be shortened by utilizing linear systems theory tools to optimize the loading profile in order to (i) reduce the time required for the sample to settle at bias strain, and (ii) utilize superposition to simultaneously quantify multiple harmonic components. Second, estimation of TIB model parameters required to assume reasonable values for ratios E_1/E_3 and v_{21}/v_{31}. Estimating all TIB model parameters without relying on such assumptions could be achieved by utilizing an analytic TIB model of order $n = 2$, as long as estimating the five parameters of its $H(s)$ from $H(j\omega_i)$ data is robust. Third, LFM accuracy can be significantly enhanced by improving the consistency and accuracy of cartilage sample preparation. Improving the flatness and parallelism of the two surfaces of cylindrical samples will enable the methodology to be applied reliably at smaller bias strains. Harvesting samples from a consistent region of cartilage can result in more repeatable results as different cartilage regions have different ECM architecture and therefore different biomechanical behavior.[27] Despite our efforts ("Materials and Methods") there is room for improvement, particularly regarding harvesting samples from more consistent cartilage regions. Finally, interpreting and validating LFM findings can be greatly enhanced by biochemical or histological characterization of the measured cartilage samples, which was not conducted here as this study focused on experimental and algorithmic development. Future work should systematically utilize histology to validate cartilage digestion by enzymes, and correlate estimated alterations on parameter estimates with observed alterations in cartilage ECM architecture.

Quantifying the biomechanical properties of tissues is essential for understanding the role of mechanical loads and extracellular matrix architecture on tissue development, physiology and pathology.[7,24,28] In this paper we presented LFM, a novel experimental alternative to the established stress-relaxation analysis for estimating the biomechanical parameters of tissues and biomaterials. Compared to stress-relaxation analysis, LFM is based on very small (0.5%) harmonic displacements and thus the properties of the samples are measured at an almost constant strain (termed the bias). Given that such tiny harmonic displacements can be applied continuously, LFM can provide real time estimates (every 1–3 h) of tissue properties. Real time monitoring of tissue permeability can provide a better alternative to standard stress-relaxation techniques that are usually prone to errors and large variance. The ability of LFM to provide estimates of biomechanical parameters at precise strain level can lead to better understanding of tissue and organ function, and can be utilized to improve the biological relevance and predictive power of tissue-level and organ-level computational models. Combined with new emerging multi-sample testing instrument designs[17] LFM can provide novel monitoring tools of tissue biomechanics. In conclusion, LFM is an alternative method for quantifying soft tissue biomechanics that can shed light on the biomechanical behavior of biomaterials, soft tissues, and tissue engineering constructs.

ACKNOWLEDGMENTS

REFERENCES

[1] Armstrong, C. G., W. M. Lai, and V. C. Mow. An analysis of the unconfined compression of articular cartilage. *J. Biomech. Eng.* 106:165–173, 1984.

[2] Ateshian, G. A., W. H. Warden, J. J. Kim, R. P. Grelsamer, and V. C. Mow. Finite deformation biphasic material properties of bovine articular cartilage from

confined compression experiments. *J. Biomech.* 30:1157–1164, 1997.

[3]Brown, T. D., and R. J. Singerman. Experimental determination of the linear biphasic constitutive coefficients of human fetal proximal femoral chondroepiphysis. *J. Biomech.* 19:597–605, 1986.

[4]Bursać, P. M., T. W. Obitz, S. R. Eisenberg, and D. Stamenović. Confined and unconfined stress relaxation of cartilage: appropriateness of a transversely isotropic analysis. *J. Biomech.* 32:1125–1130, 1999.

[5]Cohen, B., W. M. Lai, and V. C. Mow. A transversely isotropic biphasic model for unconfined compression of growth plate and chondroepiphysis. *J. Biomech. Eng.* 120:491–496, 1998.

[6]Currier, A., Q.-C. He, and P. Zysset. Conewise linear elastic materials. *J. Elasticity* 37:1–38, 1994.

[7]Engler, A. J., S. Sen, H. L. Sweeney, and D. E. Discher. Matrix elasticity directs stem cell lineage specification. *Cell* 126:677–689, 2006.

[8]Fung, Y. Biomechanics: Mechanical Properties of Living Tissues. New York: Springer, 2013.

[9]Guilak, F. Biomechanical factors in osteoarthritis. *Best Pract. Res. Clin. Rheumatol.* 25:815–823, 2011.

[10]Guilak, F., B. Fermor, F. J. Keefe, V. B. Kraus, S. A. Olson, D. S. Pisetsky, L. A. Setton, and J. B. Weinberg. The role of biomechanics and inflammation in cartilage injury and repair. *Clin. Orthop. Relat. Res.* 423:17–26, 2004.

[11]Huang, C.-Y., V. C. Mow, and G. A. Ateshian. The role of flow-independent viscoelasticity in the biphasic tensile and compressive responses of articular cartilage. *J. Biomech. Eng.* 123:410–417, 2001.

[12]June, R. K., and D. P. Fyhrie. Enzymatic digestion of articular cartilage results in viscoelasticity changes that are consistent with polymer dynamics mechanisms. *Biomed. Eng. Online* 8:32, 2009.

[13]Kiviranta, P., J. Rieppo, R. K. Korhonen, J. Julkunen, J. Toyras, and J. S. Jurvelin. Collagen network primarily controls Poisson's ratio of bovine articular cartilage in compression. *J. Orthop. Res.* 24:690–699, 2006.

[14]Laasanen, M. S., J. Toyras, R. K. Korhonen, J. Rieppo, S. Saarakkala, M. T. Nieminen, J. Hirvonen, and J. S. Jurvelin. Biomechanical properties of knee articular cartilage. *Biorheology* 40:133–140, 2003.

[15]Lai, W. M., J. S. Hou, and V. C. Mow. A triphasic theory for the swelling and deformation behaviors of articular cartilage. *J. Biomech. Eng.* 113:245–258, 1991.

[16]Lai, W. M., V. C. Mow, and V. Roth. Effects of nonlinear strain-dependent permeability and rate of compression on the stress behavior of articular cartilage. *J. Biomech. Eng.* 103:61–66, 1981.

[17]Lujan, T. J., K. M. Wirtz, C. S. Bahney, S. M. Madey, B. Johnstone, and M. Bottlang. A novel bioreactor for the dynamic stimulation and mechanical evaluation of multiple tissue-engineered constructs. *Tissue Eng. Part C* 17:367–374, 2011.

[18]Mak, A. F. The apparent viscoelastic behavior of articular cartilage—the contributions from the intrinsic matrix viscoelasticity and interstitial fluid flows. *J. Biomech. Eng.* 108:123–130, 1986.

[19]Maldonado, M., and J. Nam. The role of changes in extracellular matrix of cartilage in the presence of inflam-mation on the pathology of osteoarthritis. *Biomed. Res. Int.* 2013. doi:10.1155/2013/284873.

[20]Mansour, J. M. Biomechanics of cartilage. In: Kinesiology: The Mechanics and Pathomechanics of Human Movement, edited by C. A. Oatis. Philadelphia, PA: Lippincott Williams & Wilkins, 2003, pp. 66–79.

[21]Mow, V. C., S. C. Kuei, W. M. Lai, and C. G. Armstrong. Biphasic creep and stress relaxation of articular cartilage in compression: theory and experiments. *J. Biomech. Eng.* 102:73–84, 1980.

[22]Park, S., C. T. Hung, and G. A. Ateshian. Mechanical response of bovine articular cartilage under dynamic unconfined compression loading at physiological stress levels. *Osteoarthritis Cartilage* 12:65–73, 2004.

[23]Park, S., S. B. Nicoll, R. L. Mauck, and G. A. Ateshian. Cartilage mechanical response under dynamic compression at physiological stress levels following collagenase digestion. *Ann. Biomed. Eng.* 36:425–434, 2008.

[24]Paszek, M. J., N. Zahir, K. R. Johnson, J. N. Lakins, G. I. Rozenberg, A. Gefen, C. A. Reinhart-King, S. S. Margulies, M. Dembo, D. Boettiger, D. A. Hammer, and V. M. Weaver. Tensional homeostasis and the malignant phenotype. *Cancer Cell* 8:241–254, 2005.

[25]Sadeghi, H., D. M. Espino, and D. E. T. Shepherd. Variation in viscoelastic properties of bovine articular cartilage below, up to and above healthy gait-relevant loading frequencies. *Proc. Inst. Mech. Eng. Part H* 229:115–123, 2015.

[26]Sanchez-Adams, J., H. A. Leddy, A. L. McNulty, C. J. O'Conor, and F. Guilak. The mechanobiology of articular cartilage: bearing the burden of osteoarthritis. *Curr. Rheumatol. Rep.* 16:451, 2014.

[27]Setton, L. A., W. Zhu, and V. C. Mow. The biphasic poroviscoelastic behavior of articular cartilage: role of the surface zone in governing the compressive behavior. *J. Biomech.* 26:581–592, 1993.

[28]Soller, E. C., D. S. Tzeranis, K. Miu, P. T. C. So, and I. V. Yannas. Common features of optimal collagen scaffolds that disrupt wound contraction and enhance regeneration both in peripheral nerves and in skin. *Biomaterials* 33:4783–4791, 2012.

[29]Soltz, M. A., and G. A. Ateshian. Experimental verification and theoretical prediction of cartilage interstitial fluid pressurization at an impermeable contact interface in confined compression. *J. Biomech.* 31:927–934, 1998.

[30]Soltz, M. A., and G. A. Ateshian. A conewise linear elasticity mixture model for the analysis of tension-compression nonlinearity in articular cartilage. *J. Biomech. Eng.* 122:576–586, 2000.

[31]Soltz, M. A., and G. A. Ateshian. Interstitial fluid pressurization during confined compression cyclical loading of articular cartilage. *Ann. Biomed. Eng.* 28:150–159, 2000.

[32]Sophia Fox, A. J. A. Bedi, and S. A. Rodeo. The basic science of articular cartilage: structure, composition, and function. *Sports Health* 1:461–468, 2009.

[33]Szarko, M., K. Muldrew, and J. E. A. Bertram. Freeze-thaw treatment effects on the dynamic mechanical properties of articular cartilage. *BMC Musculoskelet. Disord.* 11:1, 2010.

[34]Tanaka, E., E. Yamano, D. A. Dalla-Bona, M. Watanabe, T. Inubushi, M. Shirakura, R. Sano, K. Takahashi, T. van Eijden, and K. Tanne. Dynamic compressive properties of the mandibular condylar cartilage. *J. Dent. Res.* 85:571–575, 2006.